



HAL
open science

Reactivity mapping of luminescence in space: Insights into heterogeneous electrochemiluminescence bioassays

Priyanka Dutta, Dongni Han, Bertrand Goudeau, Dechen Jiang, Danjun Fang, Neso Sojic

► To cite this version:

Priyanka Dutta, Dongni Han, Bertrand Goudeau, Dechen Jiang, Danjun Fang, et al.. Reactivity mapping of luminescence in space: Insights into heterogeneous electrochemiluminescence bioassays. *Biosensors & Bioelectronics*, 2020, 165, pp.112372 -. 10.1016/j.bios.2020.112372 . hal-03492323

HAL Id: hal-03492323

<https://hal.science/hal-03492323>

Submitted on 15 Jul 2022

HAL is a multi-disciplinary open access archive for the deposit and dissemination of scientific research documents, whether they are published or not. The documents may come from teaching and research institutions in France or abroad, or from public or private research centers.

L'archive ouverte pluridisciplinaire **HAL**, est destinée au dépôt et à la diffusion de documents scientifiques de niveau recherche, publiés ou non, émanant des établissements d'enseignement et de recherche français ou étrangers, des laboratoires publics ou privés.



Distributed under a Creative Commons Attribution - NonCommercial 4.0 International License

Reactivity mapping of luminescence in space: insights into heterogeneous electrochemiluminescence bioassays

Priyanka Dutta,^a Dongni Han,^{a,b} Bertrand Goudeau,^a Dechen Jiang,^c Danjun Fang,^{b,*} and Neso Sojic^{a,d,*}

^a *Univ. Bordeaux, Bordeaux INP, CNRS, UMR 5255, Site ENSCBP, 33607 Pessac, France*

^b *School of Pharmacy and Key Laboratory of Targeted Intervention of Cardiovascular Disease, Collaborative Innovation Center for Cardiovascular Disease Translational Medicine, Nanjing Medical University, Nanjing, Jiangsu 211126, China*

^c *State Key Laboratory of Analytical Chemistry for Life and School of Chemistry and Chemical Engineering, Nanjing University, Nanjing, Jiangsu, 210093, China*

^d *Department of Chemistry, South Ural State University, Chelyabinsk 454080, Russian Federation*

Corresponding authors: djf@njmu.edu.cn ; neso.sojic@enscbp.fr

Abstract

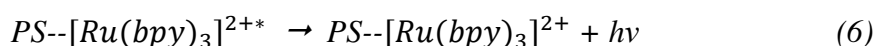
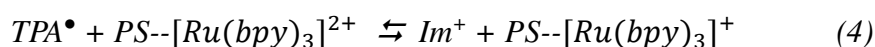
Electrochemiluminescence (ECL) is a powerful (bio)analytical method based on an optical readout. It is successfully applied in the heterogeneous format for immunoassays and imaging using the model and most widely used ECL system, which consists of the immobilized $[\text{Ru}(\text{bpy})_3]^{2+}$ label with tripropylamine (TPA) as a coreactant. However, a major drawback is the significant decrease of the ECL intensity over time. Herein, to decipher the process responsible for this progressive loss of ECL signal, we investigated its electrochemical and photophysical properties by mapping the luminescence reactivity at the level of single micrometric beads. Polystyrene beads were functionalized by the $[\text{Ru}(\text{bpy})_3]^{2+}$ dye via a sandwich immunoassay or a peptide bond. ECL emission was generated in presence of the very efficient TPA coreactant. Imaging both photoluminescence and ECL reactivities of different regions (located near or far from the electrode surface) of a $[\text{Ru}(\text{bpy})_3]^{2+}$ -decorated bead allows us to demonstrate the remarkable photophysical stability of the ECL label, even in presence of the very reactive electrogenerated TPA radicals. We show that the ECL vanishing correlates directly with the lower TPA oxidation current. Finally, we propose a simple electrochemical treatment, which allows to regenerate the electrode surface and thus to recover several times the strong initial ECL signal. The reactivity imaging approach provides insights into the ECL mechanism and the main factors governing the stability of the emission, which should find promising ECL applications in bioassays and microscopy.

Keywords: electrochemiluminescence, heterogeneous bioassays, bead-based immunoassays, electrochemistry, imaging

1. Introduction

Electrochemiluminescence (ECL) is an electrochemical process in which light is emitted by the excited state of the luminophore.(Bard 2004; Sojic 2020) The phenomenon is triggered by an initial electron-transfer reaction occurring at the electrode surface.(Hesari and Ding 2016; Hu and Xu 2010) Then, it continues by a chemical reaction between highly reactive intermediates that produces the excited state of the luminophore. Finally, it ends with its relaxation to the ground state and the photon emission. The luminophores are excited by the application of an external potential instead of a light source, which removes the possibility of background signals from scattered light and provides improved sensitivity to the detection system.(Dolci et al. 2009; Qi and Zhang 2020; Valenti et al. 2015) Controlling the applied potential provides a temporal control and better selectivity to the system.(Doeven et al. 2015; Guo et al. 2018; Li et al. 2017; Voci et al. 2020) These characteristics are the main reasons behind the fact that ECL has turned out today as a highly significant detection method in the field of analytical chemistry as well as an imaging method.(Cao et al. 2018; Ding et al. 2020; Guo et al. ; Ma et al. 2013; Marquette et al. 2003; Theakstone et al. 2019; Xu et al. 2012; Zanut et al. 2020; Zhang et al. 2019b; Zhou et al. 2015; Zhu et al. 2018) The model system involving $[\text{Ru}(\text{bpy})_3]^{2+}$ as the luminophore and tripropylamine (TPA) as the coreactant forms the basis of a large number of commercially available bead-based ECL immunoassays.(Ma et al. 2020; Qi and Zhang 2020) In heterogeneous ECL, the luminophore is immobilized on a non-conductive surface (or object) and is not directly oxidized at the electrode surface.(Habtamu et al. 2015; Miao et al. 2002; Sentic et al. 2014) Heterogeneous ECL has been widely studied over the last few decades and has found applications in a large number of immunoassays, such as tumor biomarkers, for detection of cardiac and other infectious diseases.(Blackburn et al. 1991; Muzyka 2014; Zhou et al. 2008) Such heterogeneous assays are based on non-conductive beads (e.g. polystyrene, PS) decorated with a specific capture

antibody. As in the present work, a sandwich immunoassay is formed in presence of the target analyte with the detection antibody conjugated to a $[\text{Ru}(\text{bpy})_3]^{2+}$ label (Figure 1a). (Deiss et al. 2009; Habtamu et al. 2015; Zhou et al. 2014) The remarkable sensitivity of such bead-based bioassays is due to the particular reactivity of the freely-diffusing TPA coreactant. (Miao et al. 2002; Zanut et al. 2020) Indeed, in this heterogeneous format, the labels (denoted PS-- $[\text{Ru}(\text{bpy})_3]^{2+*$), which are immobilized on the PS beads are located at micrometric distances from the electrode generate ECL and are not directly oxidized at the electrode surface. (Habtamu et al. 2015; Sentic et al. 2016; Zanut et al. 2020) The mechanism proposed can be described by the following reactions:



where Im^+ is the iminium product. (Miao et al. 2002; Qiu et al. 2016) PS-- $[\text{Ru}(\text{bpy})_3]^{2+*$ represents the ECL label bound to the PS bead.

Only the freely-diffusing coreactant TPA is oxidized at the electrode surface generating $\text{TPA}^{\bullet+}$ cation radical (reaction 2). This later deprotonates rapidly to form the neutral radical TPA^\bullet (reaction 3). Both $\text{TPA}^{\bullet+}$ and TPA^\bullet radicals diffuse over micrometric distances and react with the luminophore to generate its excited state. Indeed, TPA^\bullet is a strong reductant and reduces the immobilized PS-- $\text{Ru}(\text{bpy})_3^{2+}$ to PS-- $\text{Ru}(\text{bpy})_3^+$ (reaction 4). Then, the cation radical $\text{TPA}^{\bullet+}$ oxidizes PS-- $\text{Ru}(\text{bpy})_3^+$ to form the excited state PS-- $\text{Ru}(\text{bpy})_3^{2+*}$ (reaction 5). The excited state then deactivates by emitting a photon (reaction 6) that generates ECL. This

ECL route is the predominant pathway for such bioassays.(Miao et al. 2002) In addition, it is noteworthy that similar heterogeneous mechanism operates for ECL microscopy of cells, where the ECL labels are immobilized also on a non-conductive object (i.e. the cell membrane).(Ma et al. 2020; Valenti et al. 2017; Voci et al. 2018; Zhang et al. 2019a) Many factors affecting the light intensity and properties of ECL in such formats still remains unexplored.(Sentic et al. 2014; Valenti et al. 2016; Zanut et al. 2020) For example, a major drawback is the important decrease of the ECL intensity over time, even if this behavior is generally not mentioned or detailed in the ECL reports. However, it limits significantly the development of ECL-based microscopy and bioassays.

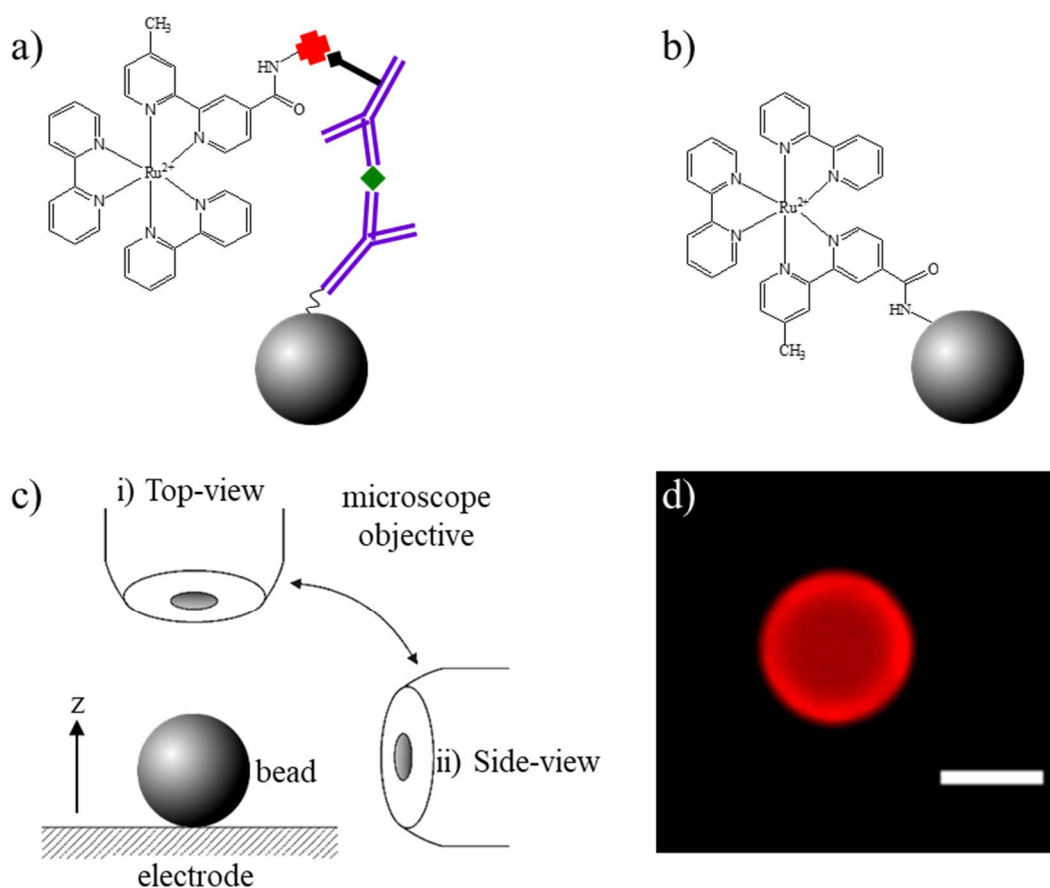


Figure 1. a) Sandwich bead-based immunoassay for interleukin 8 (IL-8) detection with ECL readout. The surface of the beads was modified with a capture antibody (anti-IL-8), the antigen (IL-8: green square), the biotinylated detection antibody (biotin: black arrow) and the

streptavidin-modified [Ru(bpy)₃]²⁺ (SA-Ru) label (streptavidin: red cross). b) PS bead functionalized with the ECL label. c) Scheme of both optical configurations used to image the labeled bead under the microscope: i) top-view and ii) side-view. d) Top-view PL image of a [Ru(bpy)₃]²⁺-decorated PS bead via sandwich immunoassay. Scale bar: 10 μm.

This work aims at investigating the effects responsible for the decrease of the light intensity in heterogeneous ECL. Such a decrease could be due either to the initial electrochemical process or to the final photophysical step. In other words, the evolution of the electrochemical and/or photophysical properties of the electrode surface or the ECL label might be involved in this signal loss. For that, we labeled the non-conductive polystyrene (PS) beads with the [Ru(bpy)₃]²⁺ complex via a sandwich immunoassay or a peptide bond and used them as the (bio)sensing platform for heterogeneous ECL studies. We mapped the photoluminescence (PL) and ECL reactivities of single PS [Ru(bpy)₃]²⁺-decorated beads using two optical configurations (Figure 1c). We showed a remarkable photophysical stability of the ECL label, even in presence of the very reactive coreactant radicals. A direct correlation of the ECL decrease with the lower TPA oxidation current is also demonstrated. The effects of very cathodic pulses on the ECL signals were then studied. This 3D imaging approach provides valuable information on the photophysical stability of the labels and on the parameters controlling the ECL signals.

2. Materials and Methods

2.1. Materials

All the reagents were purchased from Sigma-Aldrich unless otherwise noted. PS beads (radius: 6 μm) were obtained from Kisker Biotech GmbH & Co. Phosphate buffer solution

(pH 7.4, 0.1 M) was prepared by mixing 0.1 M sodium phosphate monobasic monohydrate and 0.1 M sodium phosphate dibasic heptahydrate solution with degassed solution. TPA was dissolved in PBS and the pH was adjusted to 7.4 with phosphoric acid. Capture antibody specific for interleukin 8 (IL-8), the complementary biotinylated detection antibody and IL-8 recombinant protein were obtained from R&D Systems Inc. The streptavidin-modified ruthenium complex used as a label in the immunoassay experiments was synthesized according to the procedure described by Deiss et al. (Deiss et al. 2009)

2.2. Instrumentation

The electrochemical cell was a 3-electrode system where the working electrode was glassy carbon (GC) or gold electrodes. A platinum wire was used as the counter electrode and Ag/AgCl/KCl (3M) electrode was used as the reference electrode. The experiments were performed using a μ -Autolab type III potentiostat. The PL and ECL images were recorded using an epifluorescence microscope from Leica (DMI6000, Leica Microsystems) and an Electron Multiplying Charge Coupled Device (EM-CCD 9100-13) Camera from Hamamatsu. The working electrode was placed in two different configurations inside the electrochemical cell for top-view and side-view study (Figure 1c). PL and ECL experiments were performed in PBS containing 200 mM TPA.

2.3. Immunoassay with PS beads

The PS beads were labeled with the $[\text{Ru}(\text{bpy})_3]^{2+}$ complex either via a sandwich immunoassay or via a peptide bond. In the first case, antigen storage aliquots were prepared in PBS 1x/BSA 0.1% and detection antibody storage aliquots were prepared in tris-buffered saline (TBS StartingBlock). Each washing step was done in 100 μL of TBS with 1% Tween 20. The assay was performed by incubating for 2 hours the microbeads functionalized with a capture antibody (anti-IL-8) first in a sample containing antigen (dilute to the appropriate concentration with PBS Starting Block) and washed. Then they were incubated for 30 min. in

50 μL of the biotinylated detection antibodies solution ($3\mu\text{g/mL}$ of antibody in PBS StartingBlock) and washed. Finally, the ECL label was attached to form immunocomplex by exposing the beads to a solution containing a streptavidin-modified $[\text{Ru}(\text{bpy})_3]^{2+}$ (SA-Ru) label (Figure 1a).

2.4. Functionalization of the PS beads with the ruthenium label via a peptide bond

An alternative labeling procedure based on the formation of a peptide bond was also employed to functionalize the PS beads with the $[\text{Ru}(\text{bpy})_3]^{2+}$ dye. 10 μL of beads suspension (2.5%) was washed with PBS (pH 7.4) and re-suspended in 1 mL of PBS. In the same time, 1 mg of $\text{Ru}(\text{bpy})_3^{2+}$ -NHS ester (bis(2,2'-bipyridine)-4'-methyl-4-carboxybipyridine-ruthenium N-succinimidyl ester-bis(hexafluorophosphate)) was dissolved in 100 μL of dimethyl sulfoxide and this solution was added to the beads suspension. This mixture was incubated on $+4^\circ\text{C}$ for 3 hours with continuous stirring. After the incubation the beads were washed from reaction solution with PBS 15 times by the centrifugation for 10 min at 10000 rpm to separate the beads from the solution. Finally, beads were suspended in 1 mL PBS and kept at 4°C . Figure 1b shows a functionalized bead with the $[\text{Ru}(\text{bpy})_3]^{2+}$ label via formation of amide bond. Beads were then washed for the last time and immobilized on the electrode surface for PL and/or ECL mapping.

3. Results and Discussions

PS beads were first functionalized with the $[\text{Ru}(\text{bpy})_3]^{2+}$ labels by sandwich immunoassay (Figure 1a). The surface of the microbeads was modified with a capture antibody (anti-IL-8). The beads were incubated first in a sample containing the corresponding antigen and then in a solution of biotinylated detection antibody. The final step was to attach the ECL labels by exposing the beads to a solution containing a streptavidin-modified

[Ru(bpy)₃]²⁺ complex (SA-Ru). We used beads with a 12 μm diameter in order to obtain well-resolved PL and ECL patterns. The PS--Ru(bpy)₃²⁺- modified beads were allowed to deposit on the surface of glassy carbon (GC) or Au electrodes. PL imaging of the bead modified by the sandwich immunoassay procedure was first performed under the microscope in the top-view configuration (denoted (i) in Figure 1c) in the epifluorescence mode. The PL image shows that the distribution of the ruthenium label throughout the bead is homogeneous (Figure 1d). Similar ECL and PL images and behaviors were observed for the beads functionalized with both procedures (e.g. sandwich immunoassay and amide-type reaction). Therefore, since similar PL and ECL results were obtained for both kinds of beads, we used the beads functionalized by the amide-type reaction to simplify the experimental protocol. Figure 2a-c shows a sequence of successive ECL images of the bead in the top-view configuration; the ECL signal decreases over time. ECL intensity measured over the entire bead decreased almost by a factor 3 after 30 s on GC electrode and is almost negligible after 60 s (Figure 2d). A similar behavior is observed on Au electrode but the drop of the ECL signal is even stronger with a decrease by a factor 9 after 30 s (Figure 2e). On the Au electrode, the formation of an oxide layer at the very anodic potentials required to generate ECL (Valenti et al. 2016; Zu and Bard 2000) may contribute to the decrease of the signal.

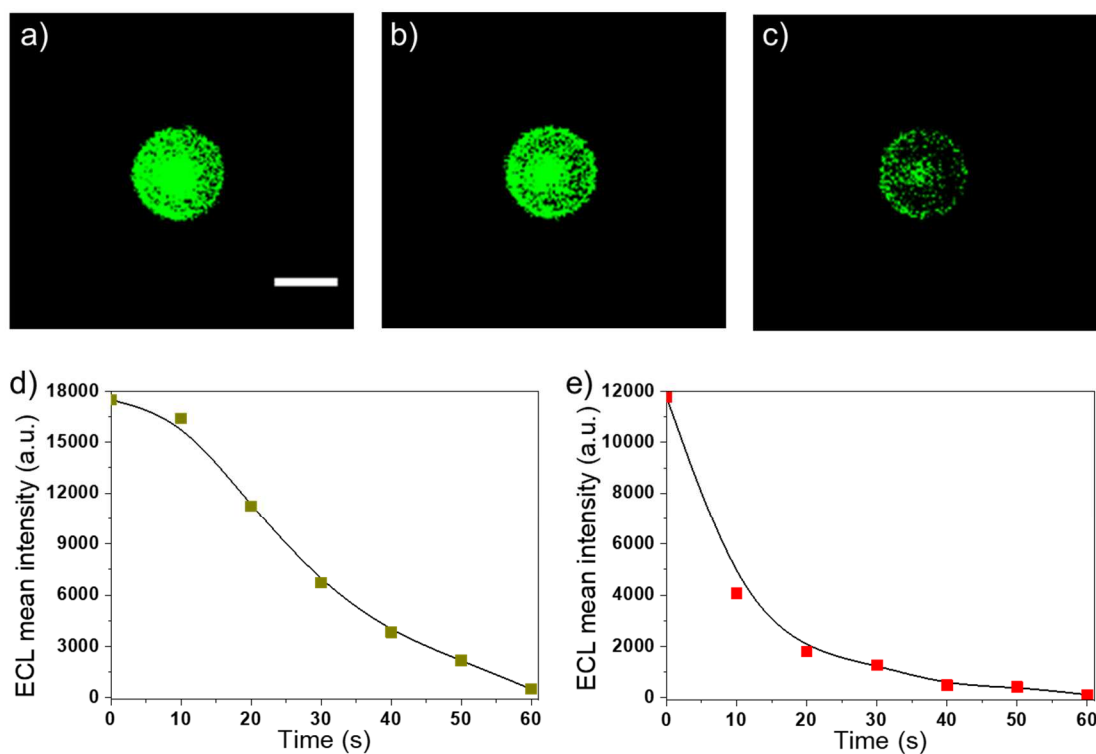


Figure 2. a-c) Sequence of successive ECL images of a single labeled bead recorded in the top-view configuration when imposing a constant potential of 1.1 V. PS 12 μm beads decorated with the ECL label were used. Exposure time: 10 s. Scale bar: 10 μm . Evolution of the ECL intensity with time on d) GC and e) gold electrode when applying a constant potential of 1.1 V. Experiments were performed with a GC or gold working electrode in a PBS solution containing 200 mM TPA (pH 7.4). Experiments have been repeated on more than 30 single beads under each set of conditions.

The top-view imaging of the bead highlights the decrease of the ECL intensity. However, this configuration does not give precise information on the PL or ECL reactivity along the axis normal to the electrode surface (i.e. z -axis on Figure 1c). To investigate the photophysical stability of the $[\text{Ru}(\text{bpy})_3]^{2+}$ label immobilized on the bead, we changed the optical configuration and the angle of observation of the ECL-emitting bead. An orthogonal side-view configuration (denoted (ii) in Figure 1c) was used to obtain a 2D mapping normal

to the electrode surface. Therefore, further studies of the labeled beads were performed in the side-view configuration. Figure 3a-c shows a sequence of PL/ECL/PL images of the same bead. The lower part of the image corresponds to the real bead and the upper part to its mirror image formed by the light reflection on the GC surface. The PL images allow precisely defining the position of the bead and its interface with the electrode. As already mentioned, the heterogeneous mechanism operating in these conditions is described by the reactions 1-6. ECL generation requires explicitly the sequential reactions of both reducing and oxidizing TPA radicals with PS-- $[\text{Ru}(\text{bpy})_3]^{2+}$ at the same location on the bead. The corresponding concentration profiles of both coreactant radicals diffusing from the electrode and around the bead were simulated previously. (Sentic et al. 2014) The spatial extension of this ECL reactive layer is confined in the first 2-3 μm height of the bead next to the electrode surface. (Sentic et al. 2014) It means that only the $[\text{Ru}(\text{bpy})_3]^{2+}$ labels located in this micrometric region close to the electrode are exposed to the actions of the TPA^\bullet and $\text{TPA}^{\bullet+}$ radicals. To study the effects of both highly oxidizing and reducing TPA radicals on the photophysical properties of the PS-- $[\text{Ru}(\text{bpy})_3]^{2+}$ labels, two regions of interest (ROI) were considered: ROI-1 is the region of the bead which is close to the electrode (i.e. $z < 3 \mu\text{m}$) whereas ROI-2 is the region located far from the electrode (i.e. $z > 3 \mu\text{m}$). In other words, ROI-1 is located in the reaction layer where TPA^\bullet and $\text{TPA}^{\bullet+}$ radicals coexist and ROI-2 can be considered as a control ROI, which is not impacted by the reactivity of the TPA radicals.

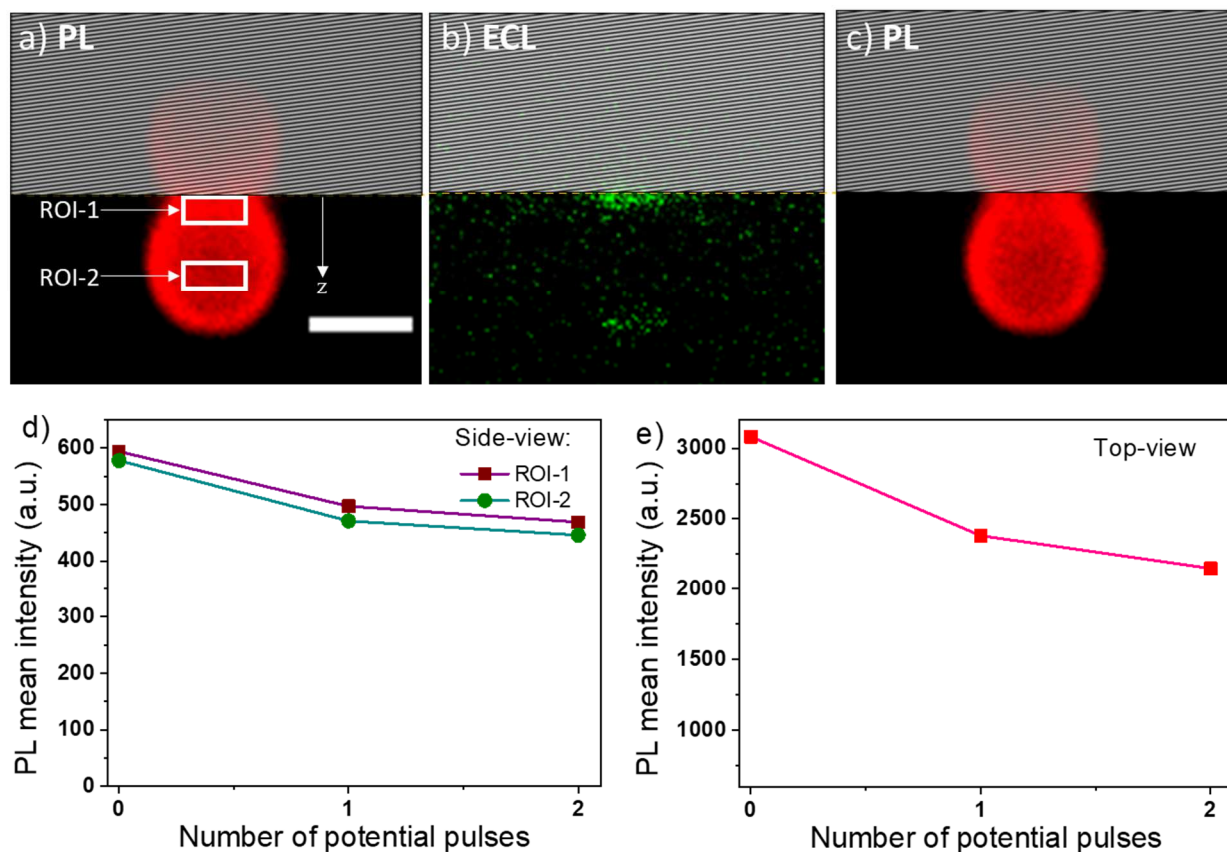


Figure 3. Side-view images of the same labeled bead in PL and ECL modes. a) PL image showing the two regions of interests (ROI-1 and ROI-2) before applying the potential pulse to the GC electrode. b) ECL image obtained when applying an anodic potential pulse of 1.1 V. c) PL image recorded after the application of the potential pulse to generate ECL. Variations of PL intensity d) in the side-view and e) top-view configurations after the application of potential pulses (1.1 V, duration: 65 s each). In the side-view configuration, the PL intensity was measured in both ROIs. Experiments were performed with a GC working electrode in a PBS solution containing 200 mM TPA (pH 7.4). The hatched zone represents the electrode surface on which light reflection occurs. The exposure times were 0.12 s and 10 s for PL and ECL images, respectively. Scale bar: 10 μm .

Using the side-view configuration, PL images of the same bead (Figures 2a and 2c) were taken before and after the generation of ECL, respectively. A potential of 1.1 V was applied for 65 s in the PBS solution containing the TPA coreactant and Figure 2b displays the corresponding first ECL image of the single functionalized bead. ECL is generated just in the region close to the electrode. As expected, it means that the labels located close to the electrode, *i.e.* in ROI-1, were exposed to both TPA[•] and TPA^{•+} radicals. On the other hand, the labels located in ROI-2 were as in the bulk and not affected by the reactions with the coreactant radicals. After one and two anodic pulses of 1.1 V for 65 s each, the PL intensity decreases with the same drop in both regions (Figure 2d). No greater decrease was observed in the region near the electrode (*i.e.* ROI-1) than far from the electrode (*i.e.* ROI-2). In the top-view configuration, a similar decrease was evidenced in the PL mode over the entire bead (Figure 2e). The same behavior was obtained on Au electrode. This PL decrease is only due to the photobleaching of the [Ru(bpy)₃]²⁺ complex during the illumination, which is required to collect the successive PL images. This study demonstrates a remarkable stability of the photophysical properties of this model label even when exposed for 1-2 minutes to strongly reactive redox radicals. It shows also that the ECL process, and in particular the initiating electrochemical step, does not affect the photophysical properties of this luminophore. Therefore, we can conclude that the observed ECL decrease is not related to an alteration of the photophysical properties of the ECL label.

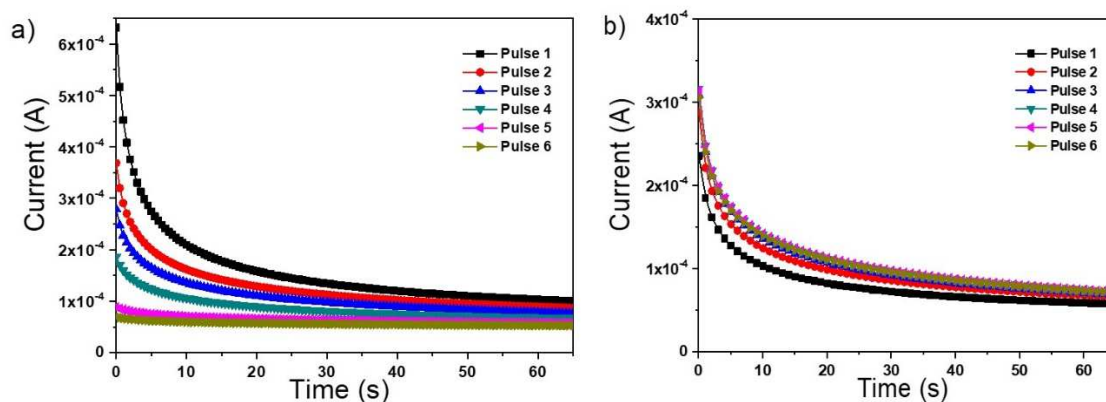


Figure 4. Successive chronoamperometric curves obtained when applying a sequence of 6 successive anodic potential pulses of 1.1 V for 65 s a) without regeneration of ECL with negative pulses and b) after regenerating the ECL by applying -2 V for 65 s between each anodic pulse. In a), we repeated 6 times the sequence: 1.1 V for 65 s; open circuit potential for 65 s. In b), we repeated 6 times the sequence: 1.1 V for 65 s; -2 V for 65 s. Only the current measured during the anodic pulses are represented. Experiments were performed with a GC working electrode in a PBS solution containing 200 mM TPA (pH 7.4).

Since the ECL labels are photochemically stable under the application of the anodic potential, we investigated then the influence of the electrochemical oxidation step on the ECL signal and its stability. The anodic current was monitored as a function of time for six successive pulses of 1.1 V for 65 s on GC electrode (Figure 4a). It shows the gradual decrease in current after each potential pulse. For example, the current measured 5 s after the application of the first potential pulse (i.e. at a time when the capacitive component becomes negligible) was 275 μ A; it decreased to \sim 200 μ A at the 2nd pulse and was just 62 μ A at the 6th pulse. Figure 5a (black bars) shows the corresponding decrease of the ECL intensity during this first sequence of 6 potential pulses. To determine the rate controlling step in the global ECL process, we plotted the variations of the ECL intensity measured on the bead in the top-

view configuration as a function of the anodic current (black curve, Figure 5b). One can observe unambiguously that both signals are cross-correlated, which demonstrated that the decrease of the observed ECL intensity is governed by the oxidation of the TPA coreactant. In other words, the decrease of the ECL intensity observed with time and successive potential pulses is due to the initiating electrochemical step. We can conclude that the electron-transfer reactions at the electrode surface, more specifically the TPA oxidation, controls the efficacy of the heterogeneous ECL process. In a previous work, we modulated the ECL response in an homogeneous format by integrating a boronic acid to the chemical structure of TPA-based coreactants, which tuned the oxidation step and thus the overall ECL intensity.(Li et al. 2016)

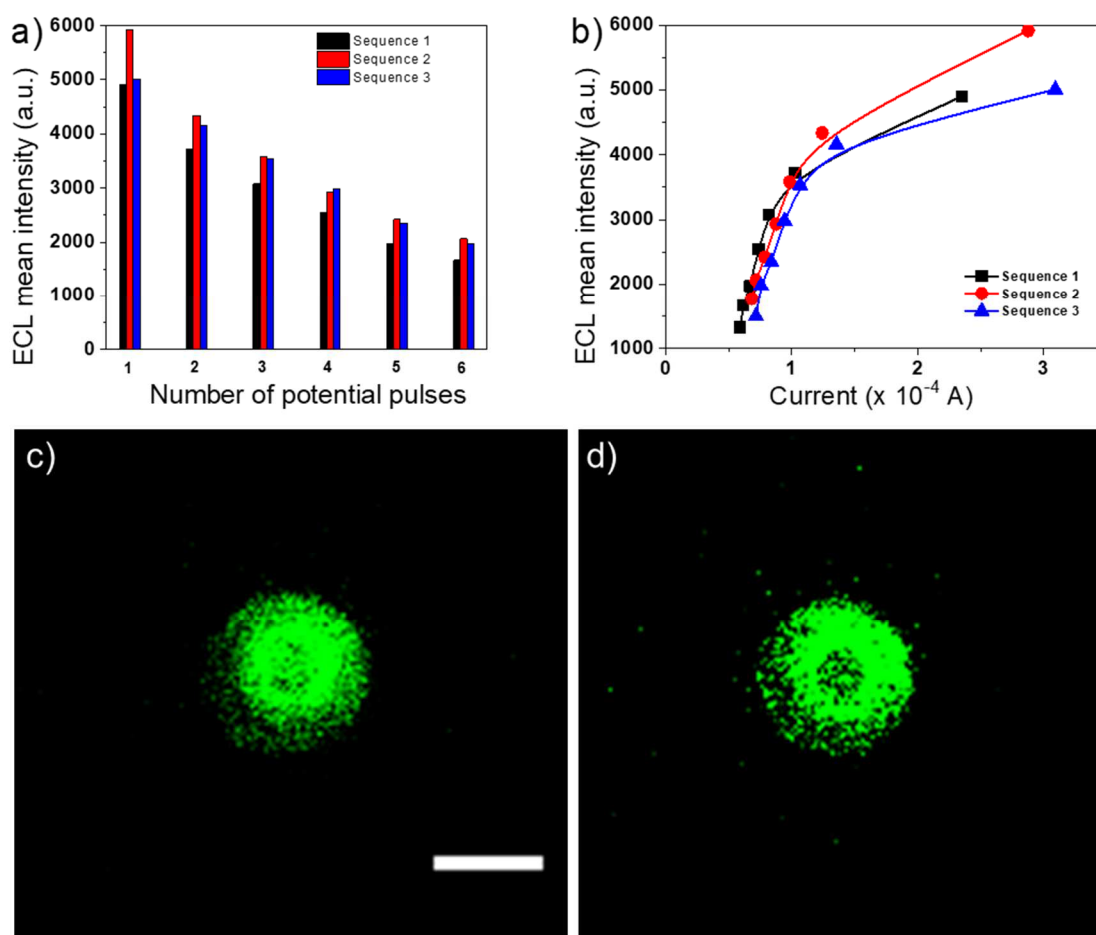


Figure 5. Effect of the application of the cathodic potential of -2 V on the ECL emission, which was generated by imposing 1.1 V. a) Variations of the ECL signal measured in the top-

view configuration when applying 3 successive sequences of 6 potential pulses of 1.1 V for 65 s. b) Cross-correlation between the ECL intensity measured during 3 sequences of 6 potential pulses of 1.1 V for 65 s and the corresponding faradaic current. After each sequence of 6 anodic potential pulses, a cathodic potential of -2 V was applied for 65 s to the GC electrode. Top-view ECL images of the same labeled bead c) before and d) after applying -2 V for 65 s. ECL emission was generated by applying a constant potential of 1.1 V. Scale bar: 10 μm . Experiments were performed in a PBS solution containing 200 mM TPA (pH 7.4).

Since electrochemistry is responsible for this progressive ECL loss, we tested different treatments of the electrode surface to regenerate the initial electrochemical properties of the GC surface. Recently, Liu and co-workers reported a drastic enhancement of the ECL of ligand-stabilized Au nanoclusters by on-electrode pre-oxidation with triethylamine coreactant.(Peng et al. 2019) The electrochemical treatment, the nature of the luminophore and the ECL processes are different from our heterogeneous work. Herein, we obtained the optimal results by applying negative potential of -2 V for 65 s. Figure 4b shows the variations of the faradaic current during a series of six successive pulses of 1.1 V for 65s on GC electrode. We imposed -2 V for 65 s between each anodic pulse. One can observe that this cathodic treatment of the electrode surface regenerated efficiently the properties of the GC surface. Indeed, the oxidation current of TPA increased in the ECL experiment, which followed the application of the cathodic pulse (Figure 4b). In fact, the anodic current recorded after this regeneration step is even stronger than the one measured during the first anodic pulse. We obtained reproducible and strong current for at least 6 successive ECL experiments. It means that this pretreatment step created functional groups on the GC surface that efficiently oxidize TPA. On the contrary, the oxidation potential required to generate ECL degrades progressively the electrochemical properties of the GC surface for the TPA

oxidation. Future works will be directed towards the identification of the chemical groups created on the electrode surface by the anodic potential and the regenerative cathodic treatment. We imaged the ECL emission of the beads before and after this regeneration step (Figure 5 c-d). ECL images revealed that we recovered the ECL pattern with this simple negative potential. It is also visible when we calculated the corresponding mean ECL intensity after the application of this cathodic potential (Figure 5a). The ECL emission of the beads could be successfully regenerated at least 6 times after applying this negative potential. Figure 5b showed a good correlation between the regeneration of the oxidation current and the ECL intensity. Finally, the restoration of ECL signals confirmed that the electrogenerated TPA radicals did not damage the photophysical properties of the ECL label and its remarkable stability in presence of highly oxidizing and reducing radicals.

4. Conclusion

In summary, heterogeneous ECL bioassays were investigated by taking single Ru(bpy)₃²⁺-decorated PS beads as the analytical platform. With two optical configurations, mapping the photoluminescence and ECL reactivities allowed deciphering the processes responsible for the significant decrease of the ECL intensity over time in heterogeneous assays using the model TPA coreactant. Photoluminescence intensity remained constant in the region close to the electrode where ECL is generated. It showed the remarkable photophysical stability of the Ru(bpy)₃²⁺ labels in presence of highly oxidizing and reducing TPA radicals electrogenerated locally. We demonstrated that the ECL vanishing is only due to the lower TPA oxidation current. Indeed, the correlation of the ECL variation with the anodic current confirmed that the oxidation step of the TPA coreactant is the one decreasing the ECL signal. We tested a simple electrochemical treatment, which allowed us to regenerate the electrode surface and thus to recover several times the strong initial ECL signal. The present study

helps in understanding several significant factors behind the complex ECL mechanism in heterogeneous bioassays. The reactivity imaging approach provides insights into the ECL mechanism and the main factors governing the stability of the emission, which should find promising applications to improve the optical readout and its reproducibility in biological and chemical sensing, new detection schemes and microscopy.

Acknowledgements

PD acknowledges the Agence Nationale de la Recherche (Neocastip ANR-15-CE09-0015-03). DH thanks the Nanjing Medical University for financial support. NS wishes to acknowledge the support from the Sino-French international research network IRN0876 (Centre National de la Recherche Scientifique, CNRS) “New nanostructured materials and biomaterials for renewable electrical energy sources” for providing facilities.

References

- Bard, A.J., 2004. *Electrogenerated Chemiluminescence*. M. Dekker, New-York.
- Blackburn, G.F., Shah, H.P., Kenten, J.H., Leland, J., Kamin, R.A., Link, J., Peterman, J., Powell, M.J., Shah, A., Talley, D.B., 1991. Electrochemiluminescence detection for development of immunoassays and DNA probe assays for clinical diagnostics. *Clin. Chem.* 37(9), 1534.
- Cao, J.-T., Wang, Y.-L., Zhang, J.-J., Dong, Y.-X., Liu, F.-R., Ren, S.-W., Liu, Y.-M., 2018. Immuno-Electrochemiluminescent Imaging of a Single Cell Based on Functional Nanoprobes of Heterogeneous Ru(bpy)₃²⁺@SiO₂/Au Nanoparticles. *Anal. Chem.* 90(17), 10334-10339.
- Deiss, F., LaFratta, C.N., Symer, M., Blicharz, T.M., Sojic, N., Walt, D.R., 2009. Multiplexed Sandwich Immunoassays using Electrochemiluminescence Imaging Resolved at the Single Bead Level. *J. Am. Chem. Soc.* 131, 6088-6089.
- Ding, H., Guo, W., Su, B., 2020. Imaging Cell-Matrix Adhesions and Collective Migration of Living Cells by Electrochemiluminescence Microscopy. *Angew. Chem. Int. Ed.* 59, 449-456.
- Doeven, E.H., Barbante, G.J., Hogan, C.F., Francis, P.S., 2015. Potential-Resolved Electrogenerated Chemiluminescence for the Selective Detection of Multiple Luminophores. *ChemPlusChem* 80(3), 456-470.
- Dolci, L.S., Zanarini, S., Ciana, L.D., Paolucci, F., Roda, A., 2009. Development of a New Device for Ultrasensitive Electrochemiluminescence Microscopy Imaging. *Anal. Chem.* 81, 6234–6241.

Guo, W., Ding, H., Gu, C., Liu, Y., Jiang, X., Su, B., Shao, Y., 2018. Potential-Resolved Multicolor Electrochemiluminescence for Multiplex Immunoassay in a Single Sample. *J. Am. Chem. Soc.* 140(46), 15904-15915.

Habtamu, H.B., Sentic, M., Silvestrini, M., De Leo, L., Not, T., Arbault, S., Manojlovic, D., Sojic, N., Ugo, P., 2015. A sensitive electrochemiluminescence immunosensor for celiac disease diagnosis based on nanoelectrode ensembles. *Anal. Chem.* 87, 12080–12087.

Hesari, M., Ding, Z., 2016. Review—Electrogenerated Chemiluminescence: Light Years Ahead. *J. Electrochem. Soc.* 163(4), H3116-H3131.

Hu, L., Xu, G., 2010. Applications and trends in electrochemiluminescence. *Chem. Soc. Rev.* 39(8), 3275-3304.

Li, H., Bouffier, L., Arbault, S., Kuhn, A., Hogan, C.F., Sojic, N., 2017. Spatially-resolved multicolor bipolar electrochemiluminescence. *Electrochem. Commun.* 77, 10-13.

Li, H., Sedgwick, A.C., Li, M., Blackburn, R.A.R., Bull, S.D., Arbault, S., James, T.D., Sojic, N., 2016. Selective electrochemiluminescent sensing of saccharides using boronic acid-modified coreactant. *Chem. Commun.* 52(87), 12845-12848.

Ma, C., Cao, Y., Gou, X., Zhu, J.-J., 2020. Recent Progress in Electrochemiluminescence Sensing and Imaging. *Anal. Chem.* 92(1), 431-454.

Ma, G., Zhou, J., Tian, C., Jiang, D., Fang, D., Chen, H., 2013. Luminol Electrochemiluminescence for the Analysis of Active Cholesterol at the Plasma Membrane in Single Mammalian Cells. *Anal. Chem.* 85(8), 3912-3917.

Marquette, C.A., Degiuli, A., Blum, L.J., 2003. Electrochemiluminescent biosensors array for the concomitant detection of choline, glucose, glutamate, lactate, lysine and urate. *Biosens. Bioelectron.* 19, 433-439.

Miao, W., Choi, J.-P., Bard, A.J., 2002. Electrogenerated Chemiluminescence 69: The Tris(2,2'-bipyridine)ruthenium(II), (Ru(bpy)₃²⁺)/Tri-n-propylamine (TPrA) System Revisited A New Route Involving TPrA^{•+} Cation Radicals. *J. Am. Chem. Soc.* 124, 14478-14485.

Muzyka, K., 2014. Current trends in the development of the electrochemiluminescent immunosensors. *Biosens. Bioelectron.* 54, 393-407.

Peng, H., Huang, Z., Sheng, Y., Zhang, X., Deng, H., Chen, W., Liu, J., 2019. Pre-oxidation of Gold Nanoclusters Results in a 66 % Anodic Electrochemiluminescence Yield and Drives Mechanistic Insights. *Angew. Chem. Int. Ed.* 58(34), 11691-11694.

Qi, H., Zhang, C., 2020. Electrogenerated Chemiluminescence Biosensing. *Anal. Chem.* 92(1), 524-534.

Qiu, R., Zhang, X., Luo, H., Shao, Y., 2016. Mass spectrometric snapshots for electrochemical reactions. *Chem. Sci.* 7(11), 6684-6688.

Sentic, M., Milutinovic, M., Kanoufi, F., Manojlovic, D., Arbault, S., Sojic, N., 2014. Mapping electrogenerated chemiluminescence reactivity in space: mechanistic insight into model systems used in immunoassays. *Chem. Sci.* 5(6), 2568-2572.

Sentic, M., Virgilio, F., Zanut, A., Manojlovic, D., Arbault, S., Tormen, M., Sojic, N., Ugo, P., 2016. Microscopic imaging and tuning of electrogenerated chemiluminescence with boron-doped diamond nanoelectrode arrays. *Anal. Bioanal. Chem.* 408(25), 7085-7094.

Sojic, N., 2020. Analytical Electrogenerated Chemiluminescence: From Fundamentals to Bioassays. Royal Society of Chemistry (RSC) Publishing.

Theakstone, A.G., Doeven, E.H., Conlan, X.A., Dennany, L., Francis, P.S., 2019. 'Cathodic' electrochemiluminescence of [Ru(bpy)₃]²⁺ and tri-n-propylamine confirmed as emission at the counter electrode. *Chem. Commun.* 55, 7081-7084.

Valenti, G., Fiorani, A., Li, H., Sojic, N., Paolucci, F., 2016. Essential Role of Electrode Materials in Electrochemiluminescence Applications. *ChemElectroChem* 3(12), 1990-1997.

Valenti, G., Scarabino, S., Goudeau, B., Lesch, A., Jović, M., Villani, E., Sentic, M., Rapino, S., Arbault, S., Paolucci, F., Sojic, N., 2017. Single Cell Electrochemiluminescence Imaging: From the Proof-of-Concept to Disposable Device-Based Analysis. *J. Am. Chem. Soc.* 139(46), 16830-16837.

Valenti, G., Zangheri, M., Sansaloni, S.E., Mirasoli, M., Penicaud, A., Roda, A., Paolucci, F., 2015. Transparent Carbon Nanotube Network for Efficient Electrochemiluminescence Devices. *Chem. Eur. J.* 21(36), 12640-12645.

Voci, S., Duwald, R., Grass, S., Hayne, D.J., Bouffier, L., Francis, P.S., Lacour, J., Sojic, N., 2020. Self-enhanced multicolor electrochemiluminescence by competitive electron-transfer processes. *Chem. Sci.*

Voci, S., Goudeau, B., Valenti, G., Lesch, A., Jović, M., Rapino, S., Paolucci, F., Arbault, S., Sojic, N., 2018. Surface-Confined Electrochemiluminescence Microscopy of Cell Membranes. *J. Am. Chem. Soc.* 140(44), 14753-14760.

Xu, L., Li, Y., Wu, S., Liu, X., Su, B., 2012. Imaging Latent Fingerprints by Electrochemiluminescence. *Angew. Chem. Int. Ed.* 51(32), 8068-8072.

Zanut, A., Fiorani, A., Canola, S., Saito, T., Ziebart, N., Rapino, S., Rebecani, S., Barbon, A., Irie, T., Josel, H.-P., Negri, F., Marcaccio, M., Windfuhr, M., Imai, K., Valenti, G., Paolucci, F., 2020. Insights into the mechanism of coreactant electrochemiluminescence facilitating enhanced bioanalytical performance. *Nature Communications* 11(1), 2668.

Zhang, J., Arbault, S., Sojic, N., Jiang, D., 2019a. Electrochemiluminescence Imaging for Bioanalysis. *Annu. Rev. Anal. Chem.* 12(1), 275-295.

Zhang, J., Jin, R., Jiang, D., Chen, H.-Y., 2019b. Electrochemiluminescence-Based Capacitance Microscopy for Label-Free Imaging of Antigens on the Cellular Plasma Membrane. *J. Am. Chem. Soc.* 141(26), 10294-10299.

Zhou, J., Ma, G., Chen, Y., Fang, D., Jiang, D., Chen, H.-y., 2015. Electrochemiluminescence Imaging for Parallel Single-Cell Analysis of Active Membrane Cholesterol. *Anal. Chem.* 87(16), 8138-8143.

Zhou, X., Xing, D., Zhu, D., Jia, L., 2008. Magnetic beads-based electrochemiluminescence assay for rapid and sensitive detection of telomerase activity. *Electrochem. Commun.* 10(4), 564-567.

Zhou, X., Zhu, D., Liao, Y., Liu, W., Liu, H., Ma, Z., Xing, D., 2014. Synthesis, labeling and bioanalytical applications of a tris(2,2'-bipyridyl)ruthenium(II)-based electrochemiluminescence probe. *Nat. Protocols* 9(5), 1146-1159.

Zhu, M.-J., Pan, J.-B., Wu, Z.-Q., Gao, X.-Y., Zhao, W., Xia, X.-H., Xu, J.-J., Chen, H.-Y., 2018. Electrogenated Chemiluminescence Imaging of Electrocatalysis at a Single Au/Pt Janus Nanoparticle. *Angew. Chem. Int. Ed* 57(15), 4010-4014.

Zu, Y., Bard, A.J., 2000. Electrogenated chemiluminescence. 66. The role of direct coreactant oxidation in the ruthenium tris(2,2')bipyridyl/triethylamine system and the effect of halide ions on the emission intensity. *Anal. Chem.* 72, 3223-3232.